

Restorer: Solving Multiple Image Restoration Tasks with One Set of Parameters

Jiawei Mao¹, Xuesong Yin¹, and Yuanqi Chang¹

Hangzhou Dianzi University,
211330013, yinxs, 211330020@hdu.edu.cn

Abstract. Although there are many excellent solutions in image restoration, the fact that they are specifically designed for a single image restoration task may prevent them from being state-of-the-art (SOTA) in other types of image restoration tasks. While some approaches require considering multiple image restoration tasks, they are still not sufficient for the requirements of the real world and may suffer from the task confusion issue. In this work, we focus on designing a unified and effective solution for multiple image restoration tasks including deraining, desnowing, defogging, deblurring, denoising, and low-light enhancement. Based on the above purpose, we propose a Transformer network Restorer with U-Net architecture. In order to effectively deal with degraded information in multiple image restoration tasks, we need a more comprehensive attention mechanism. Thus, we design all-axis attention (AAA) through stereo embedding and 3D convolution, which can simultaneously model the long-range dependencies in both spatial and channel dimensions, capturing potential correlations among all axis. Moreover, we propose a Restorer based on textual prompts. Compared to previous methods that employ learnable queries, textual prompts bring explicit task priors to solve the task confusion issue arising from learnable queries and introduce interactivity. Based on these designs, Restorer demonstrates SOTA or comparable performance in multiple image restoration tasks compared to universal image restoration frameworks and methods specifically designed for these individual tasks. Meanwhile, Restorer is faster during inference. The above results along with the real-world test results show that Restorer has the potential to serve as a backbone for multiple real-world image restoration tasks.

Keywords: Image Restoration · Severe Weather Removal · Textual Prompt

1 Introduction

Environments such as severe weather (rain, fog, and snow) and low light can reduce image visibility. Cameras produce issues such as noise and blurring when shooting. All these negative factors dramatically affect many computer vision algorithms especially object detection, semantic segmentation, and depth estimation which are crucial components of surveillance systems, autonomous vehicle

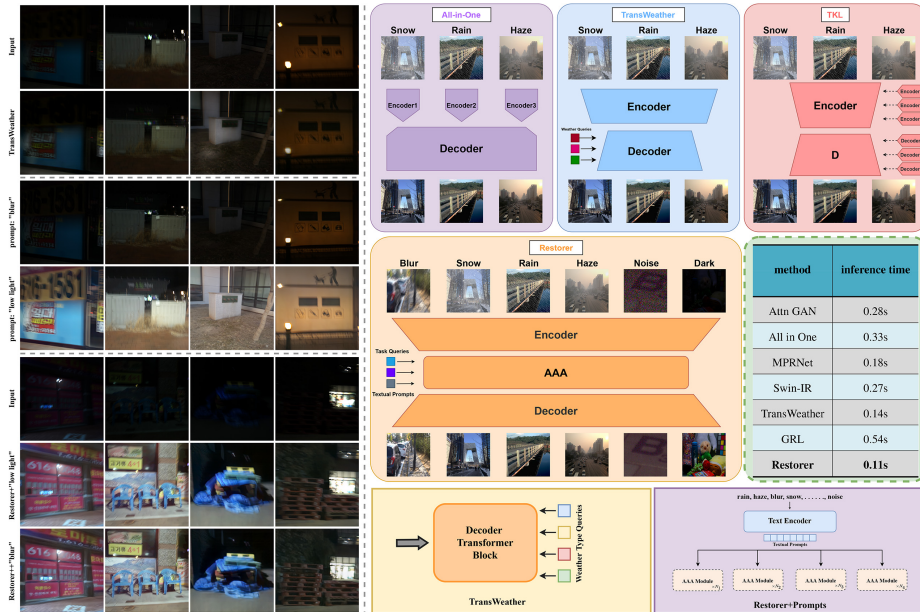


Fig. 1: Overview of existing all-in-one image restoration methods and Restored images of TransWeather and Restorer based on different textual prompts on the RealBlur dataset. Restorer achieves promising performance in more image restoration tasks with shorter inference time. TransWeather confuses the low-light enhancement task when performing the deblurring task, resulting in poor deblurring results. In contrast, Restorer at different textual prompts strictly performed the corresponding image restoration task.

systems, or edge devices [37, 42–44]. This appears to be particularly important for image restoration tasks for these degradations.

To tackle these tasks, various image restoration algorithms like image deraining [17, 49, 65], desnowing [8, 38, 73], defogging [12, 45, 63], deblurring [29, 41, 74], denoising [22, 48, 72], and low-light image enhancement [15, 60] have been widely explored nowadays. Despite their promising performance, they may not be optimal in other types of image restoration tasks because they are specifically designed for a single type of degradation. A simple idea is to switch between a range of different types of image restoration algorithms. However, this is undoubtedly costly. Li et al. [35] searched for appropriate weights in several severe weather frameworks with neural architecture search (NAS) technique to address this issue. Although this approach has achieved better or comparable results in several severe weather image restoration tasks, it requires multiple encoders to be selected based on the type of image restoration task, making it inefficient. To address the above issue, Chen et al. [9] proposed a single encoder framework TKL through two-stage knowledge distillation and multi-contrastive regularization achieving promising results on different severe weather image restoration tasks simultaneously. Valanarasu et al. [56] proposed TransWeather, a Trans-

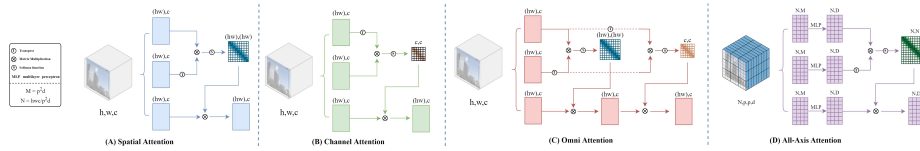


Fig. 2: Illustration of spatial attention, channel attention, omni self-attention, and all-axis attention.

former network with only one encoder and one decoder, which adapts to a specific severe weather image restoration task by learnable weather type embeddings.

Although TransWeather and TKL achieve encouraging results in different types of image restoration tasks, they are still insufficient for the requirements of real-world applications because degradations such as low light, noise, and blurring in the real world also affect the computer vision algorithm performance. Meanwhile, it is complex for TKL to find multiple appropriate specific task image restoration models for two-stage distillation. While TransWeather works well in spatially removing weather degradation at different scales, its network design ignores channel information that is equally important for image restoration tasks resulting in its performance still falling short on some image restoration tasks. Furthermore, the learnable weather type embeddings in Transweather lack interpretability and clear definitions. This may lead to confusion between different image restoration tasks (see Figure 9).

In this work, we propose the Transformer network Restorer with U-Net [51] architecture to face the above challenges. It can efficiently address multiple image restoration tasks including image deraining, desnowing, defogging, deblurring, denoising, and low-light image enhancement. To handle the different degradation information in image restoration tasks mentioned above, Restorer’s Transformer module needs a more comprehensive attention mechanism. Thus, we propose the all-axis attention (AAA) module in Restorer by design of stereo embedding and 3D convolution. All channels of the feature map in spatial attention share the attention weights obtained by calculating the cross-covariance of the spatial directions. This attention modeling scheme ignores the channel information in the feature map. However, [58, 68] experimental results show that attention modeling schemes for channel dimensions are also crucial in image restoration tasks, they are computationally more compact than spatial attention. Pixels on all spaces in the channel attention modeling scheme share channel attention weights. This scheme ignores spatial information, leading to a significant reduction in relation modeling capability impairing model performance. Our AAA extends the interaction to 3D space, fulfilling the complementary strengths of these two attention modeling schemes. Thus, AAA is more suitable for handling multiple image restoration tasks. In addition, we introduce learnable task queries in AAA to predict task-related degenerate feature vectors. In order to preserve the fine details in the stereo patches, we also design a 3D deep convolutional feed-forward network (3D-DCFFN) for the stereo patches in the AAA module to perform local modeling of the stereo patches in both space and channel at once. Experiments show that 3D-DCFFN facilitates Restorer to obtain high-

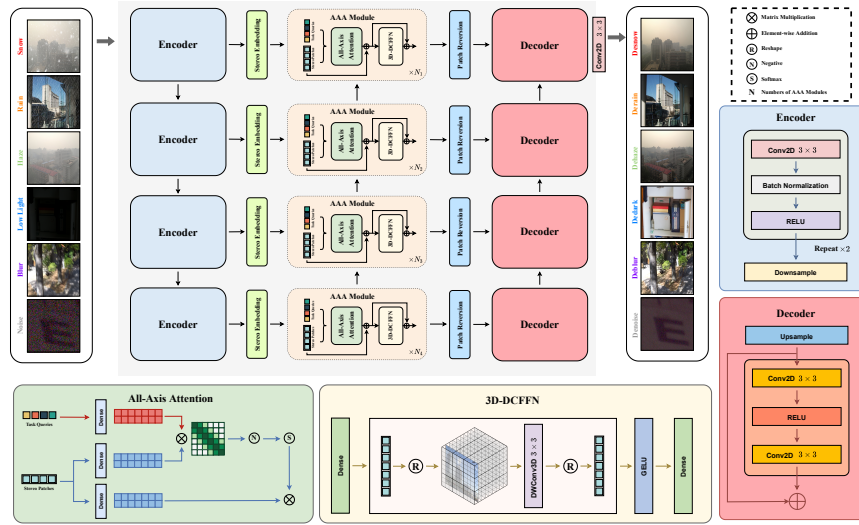


Fig. 3: The overall architecture of the proposed Restorer and the structure of each Restorer component. The upsampling and downsampling operations are realized by transposed convolution and convolution with a stride of 2, respectively.

fidelity restored images. To address the task confusion issue caused by learnable task queries, we propose a version of Restorer based on textual prompts. Compared to learnable task queries that lack interpretability, textual prompts have a deterministic task prior thus effectively solving the task confusion issue and introducing interactivity for Restorer to let the user decide what to restore for the image. Additionally, we find that Restorer with text prompts also solves the issue of multiple degradations in the same image.

Experiments on numerous standard datasets show that Restorer achieves state-of-the-art (SOTA) or competitive results on multiple image restoration tasks compared to universal image restoration frameworks and methods specifically designed for these individual tasks. Meanwhile, the results on the real-world dataset show that Restorer is robust enough. Figure 9 indicates that Restorer is more favorable in efficiency. These results together demonstrate the potential of Restorer as a real-world application for image restoration tasks.

2 Related Work

2.1 Universal Image Restoration Tasks

Zamir et al. [70] proposed MPRNet with a multi-stage architecture, which utilizes in-situ supervised attention to progressively learn the restoration function for degraded inputs. Mou et al. [39] integrated a gradient estimation strategy into the gradient descent step of the Proximal Gradient Descent (PGD) algorithm to propose DGUNet for the image restoration task. The Uformer proposed by Wang et al. [61] has achieved success in image restoration through the design

of a localized enhancement window transformer structure. Tu et al. [55] proposed MAXIM, the first general-purpose MLP architecture for low-level vision, which is more efficient and flexible in image restoration tasks. Chen et al. [6] proposed a simple baseline NAFNet for the image restoration task through extensive network design experiments. Li et al. [36] proposed GRL performing image restoration tasks that achieve a balance between the spatial and temporal complexity and modeling capabilities of self-attention through the design of anchored stripe self-attention.

Although these methods achieve satisfactory image restoration results, however, degradation residuals may exist not only in the feature map space dimension but also in the channel dimension when performing image restoration tasks. This means that image restoration needs to consider both spatial and channel modeling, especially for unified image restoration models for multiple low-level visual tasks. While some work [58] has explored this, they typically employ two stages of modeling for both space and channel, and this asynchrony from different stages prevents image restoration algorithms from fully exploiting potential correlations between all axis of a degraded image. Thus, the stereo spatial attention design that combines channel dimensions in the AAA Module is better suited to the requirements of a unified image restoration task.

2.2 All-in-One Image Restoration Tasks

Li et al. [35] designed All in One for image restoration with a scheme of neural architecture search (NAS) and adversarial training based on classification. However, All in One requires multiple specific encoders to be selected based on the type of degradation, which definitely affects the efficiency. To address this problem, Valanarasu et al. [56] were inspired by DETR [3] to design transformers with learnable weather type embeddings to adapt to the weather degradation at hand. Chen et al. [9] learned crucial features for different types of degradation from multiple encoders through two-stage knowledge distillation and multi-contrast knowledge regularization. Li et al. [34] restored various degraded images in a single network by contrastive-based degradation encoder and degradation-guided restoration network.

The main challenge of current unified image restoration methods lies in the mutual interference between different tasks, while contrastive learning and learnable weather type embeddings can alleviate this issue to a certain extent, in some composite degradation scenes (e.g., low-light blurring scenes), the interference between different tasks will be more serious, which may lead to the failure of these designs (see Figure 9). The introduction of text prompts in Restorer is a favorable solution to the above problem. Users can explicitly perform specific image restoration tasks by instructing the model, thus eliminating interference between tasks. In addition, Restorer can remove compound degradation in real scenes based on iterative prompts.

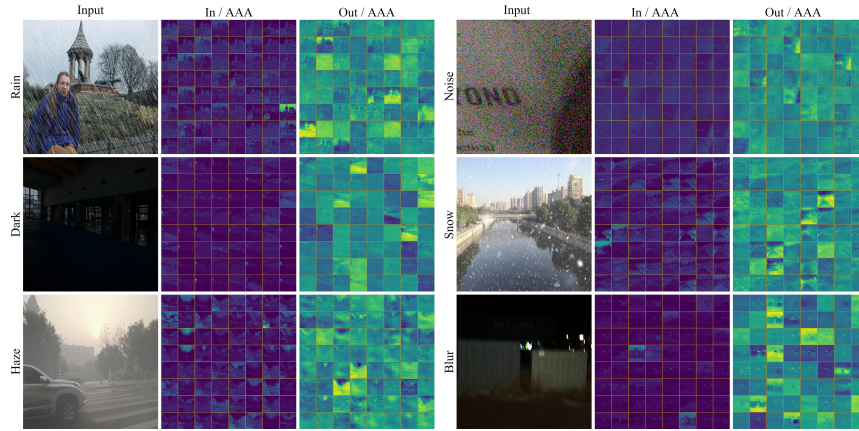


Fig. 4: Visualization of feature maps for each channel before and after the AAA module for different image restoration tasks. It can be observed that there are significant degradation residuals in the inter-channel feature maps before the AAA module, while the degradation residuals among the channels are eliminated after the AAA module. Please zoom in to see the details better.

3 Proposed Method

Our main goal is to develop an efficient Transformer model that meets the needs of real-world image restoration, which can be quickly applied to multiple image restoration tasks. In this section, we first describe the overall pipeline of Restorer (see Figure 3). Then, we discuss the core components related to the all-axis attention module in Restorer: the stereo embedding, the all-axis attention, 3D deep convolutional feedforward networks, and Restorer based on textual prompts. Finally, we introduce the loss function.

3.1 Overall Pipeline

Given a degraded image, Restorer transforms it from low-level features to high-level features via four-level symmetric encoder-AAA-decoder architecture. As shown in Figure 3, Restorer’s encoder uses a compact convolutional architecture to extract low-level feature embeddings for computational efficiency. The design of the encoder-AAA-decoder in different stages guarantees Restorer’s ability to effectively capture visual information at different granularities like U-Net [51]. For different stages of the encoder output, we first transform it into a sequence of stereo token embeddings by stereo embedding. Then AAA mines potential dependencies between the learnable task queries representing task-related degraded feature vectors and the degraded feature in the all-axis based on stereo patches and filters out the degenerate features from the feature embedding in both spatial and channel dimensions via negative affinity matrices. Next, the AAA module performs fine-grained feature extraction of stereo patches through 3D-DCFFN to preserve the high-frequency information in the image. For the

stereo patch output from the AAA module, the convolutional decoder converts them into feature maps through the patch reversion layer and progressively restores a high-resolution representation by stacked convolution and transposed convolution while preserving the fine details of the image. Convolution has a natural advantage over Transformer in local modeling. Eventually, a high-fidelity restored image is obtained from the 3×3 convolutional projection block.

3.2 All-Axis Attention Module

As illustrated in Figure 2, the one-dimensional attention operator is limited by space or channel dimension thus failing to exploit the full potential of the attention mechanism in image restoration tasks. For the spatial attention operator [5, 57], since the channels share the same spatial weights, it can only mine potential correlations in the degraded image space, ignoring the explicit use of channel information. Recent studies [58, 68] have shown that the channel attention operator is more compact than the spatial attention operator, it also plays an important role in image restoration tasks. However, the channel attention operator ignores critical spatial information in the image restoration task leading to a drastic reduction in the relational modeling capability compromising the accuracy of aggregation (see Figure 6), especially for unified image restoration tasks. Although Wang et al. proposed OSA [58] to lift the limitation of the one-dimensional attention operator, this approach requires two stages of modeling through both spatial attention and channel attention. This asynchrony prevents OSA from fully mining the potential dependencies between the all-axis of degraded images. In contrast, our AAA truly extends the interaction to 3D space through stereo embedding, which enjoys the complementary spatial and channel advantages of the one-dimensional attention operator, making it more suitable for image restoration tasks.

Stereo Embedding. For the AAA module in different stages, Restorer employs stereo embedding to divide the feature map $F \in \mathbb{R}^{h \times w \times c}$ ($h \times w$ denotes the spatial dimension and c denotes the number of channels) into stereo token embeddings. Specially, the stereo embedding first reshapes the feature map into a sequence of stereo tokens $E \in \mathbb{R}^{p \times p \times d \times (n_p^2 n_d)}$; where p^2 and d denote the stereo token space dimension and the channel dimension, respectively, $N = n_p \times n_p \times n_d = hwc/p^2d$ is the resulting number of stereo tokens. The stereo embedding then replaces the time dimension in the 3D convolution with the channel dimension to map the stereo token, thus introducing stereo spatial information for each stereo token. Next, we flatten the stereo token sequence and project it to a constant potential vector size D with linear layer to obtain the stereo token embeddings $E \in \mathbb{R}^{N \times D}$ like ViT [14]. To stabilize the learning process and improve convergence during training, the stereo embedding is treated with layer normalization [2] for stereo token embeddings. Finally, we add learnable position embeddings E_{pos} for stereo token embeddings to preserve stereo position information (see Equation 1). Compared to other token embedding division ways, stereo token embeddings divided in 3D space allow for the modeling

of long-range dependencies in both space and channel through attention.

$$\begin{aligned}
\mathbf{F} &= [\mathbf{f}^{(1)}; \mathbf{f}^{(2)}; \dots; \mathbf{f}^{(i)}; \dots; \mathbf{f}^{(N)}], \mathbf{f}^{(i)} \in \mathbb{R}^{p \times p \times d}, \\
\mathbf{Z} &= \text{Flat}(\text{3DConv}(\mathbf{F})), \\
\mathbf{Z} &= [\mathbf{z}^{(1)}\mathbf{W}; \mathbf{z}^{(2)}\mathbf{W}; \dots; \mathbf{z}^{(i)}\mathbf{W}; \dots; \mathbf{z}^{(N)}\mathbf{W}], \mathbf{z}^{(i)} \in \mathbb{R}^{p^2 d}, \mathbf{W} \in \mathbb{R}^{(p^2 d) \times D}, \\
\mathbf{Z} &= \text{LN}(\mathbf{Z}) + \mathbf{E}_{\text{pos}}, \mathbf{E}_{\text{pos}} \in \mathbb{R}^{N \times D},
\end{aligned} \tag{1}$$

where $\text{3DConv}(\cdot)$ denotes 3D convolution, $\text{Flat}(\cdot)$ is the flattening operation, \mathbf{W} is the linear layer weights, and $\text{LN}(\cdot)$ is the layer normalization operation.

All-Axis Attention. For the stereo patches $\mathbf{z} \in \mathbb{R}^{N \times D}$ obtained by stereo token embeddings, we perform a multi-head attention computation between them and the learnable task queries $\mathbf{t} \in \mathbb{R}^{N \times D}$ used to fit the task-related degenerate feature vectors:

$$\begin{aligned}
\mathbf{q} &= \mathbf{t}\mathbf{W}_q, \mathbf{k} = \mathbf{z}\mathbf{W}_k, \mathbf{v} = \mathbf{z}\mathbf{W}_v, \\
\mathbf{o}^{(n)} &= \theta(0 - \mathbf{q}^{(n)}\mathbf{k}^{(n)\top} / \sqrt{d})\mathbf{v}^{(n)}, n = 1, \dots, H, \\
\mathbf{o} &= [\mathbf{o}^{(1)}; \dots; \mathbf{o}^{(H)}]\mathbf{W}_o,
\end{aligned} \tag{2}$$

where $\mathbf{W}_q, \mathbf{W}_k, \mathbf{W}_v, \mathbf{W}_o$ represent the mapping matrices, respectively. H indicates the number of heads. $\theta(\cdot)$ is a softmax function, and d is the embedding dimension of each header to avoid gradient vanishing. Unlike vanilla multi-head attention, AAA adopts negative affinity matrices. Based on these negative affinity matrices, the Restorer can assign attention weights that are not related to the degradation in all axis through latent dependencies between the learnable task queries and the stereo patches thus effectively removing the degradation information from the stereo patches in both spatial and channel (see Figure 4). In addition, to further enhance the robustness of AAA to scale, we have also established connections for AAA modules at different stages.

3D Deep Convolutional Feedforward Networks. A Feedforward network with deep convolution facilitates Transformer to extract fine-grained features. This contributes to the restoration image retaining the fine details in the input image thus the AAA module designs the 3D deep convolutional feedforward network (3D-DCFFN). Unlike other work on convolutional feedforward networks [19, 20, 24], the 3D-DCFFN in our work does not capture the local information of the whole feature map but rather the fine-grained features of each stereo token. In contrast, convolution acting on a feature map may lack sensitivity to fine-grained location information to some extent. Therefore, for image restoration tasks that emphasize fine restoration of exact locations, 3D-DCFFN may be more suitable. Meanwhile, 3D-DCFFN not only considers the spatial information in the tokens but also pays attention to the channel information of the tokens at the same time, which has not been concerned by previous work. First, we map the AAA output to the hidden dimensions with a linear layer and reshape it back to stereo tokens $\mathbf{E} \in \mathbb{R}^{p \times p \times d \times (n_p^2 n_d)}$. For stereo tokens, we use 3D deep convolution to extract fine-grained features in 3D space. Finally, 3D-DCFFN reshapes the stereo tokens back to 2D stereo patches and maps them

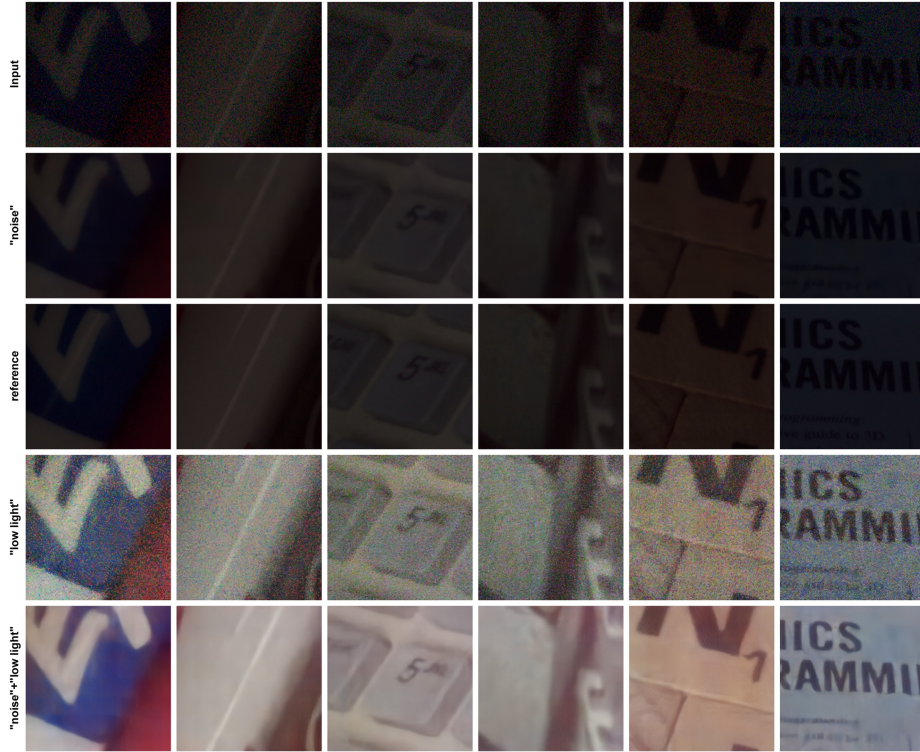


Fig. 5: Restorer’s image restoration results at different textual prompts on SIDD.

back to the input dimensions by linear layer. Appendix D indicates that the 3D-DCFFN based on the above design effectively improves the quality of restored images by performing local modeling of the stereo patches in both spatial and channel dimensions.

3.3 Restorer based on textual prompts

Although TransWeather has shown satisfactory results in multiple severe weather image restoration tasks, the lack of a clear definition of learnable task queries makes it difficult to achieve an accurate distinction between image restoration task types in the face of various degradations leading to task confusion issue. To address this issue, we propose Restorer based on textual task prompts. Specifically, we represent degraded types of text (e.g., "low light", "rain", "blur", etc.) with the text encoder from CLIP [47] to obtain textual prompts. Textual prompts would replace learnable task queries into the AAA module for each stage of Restorer. As shown in Figure 9, compared with learnable task queries, this textual prompt with the task prior provides clear instructions for Restorer’s image restoration effectively solving the task confusion issue caused by learnable task queries thus further improving Restorer’s performance in each image restoration task. At the same time, textual prompts introduce significant interactivity into Restorer, allowing the user to decide what restoration tasks need to

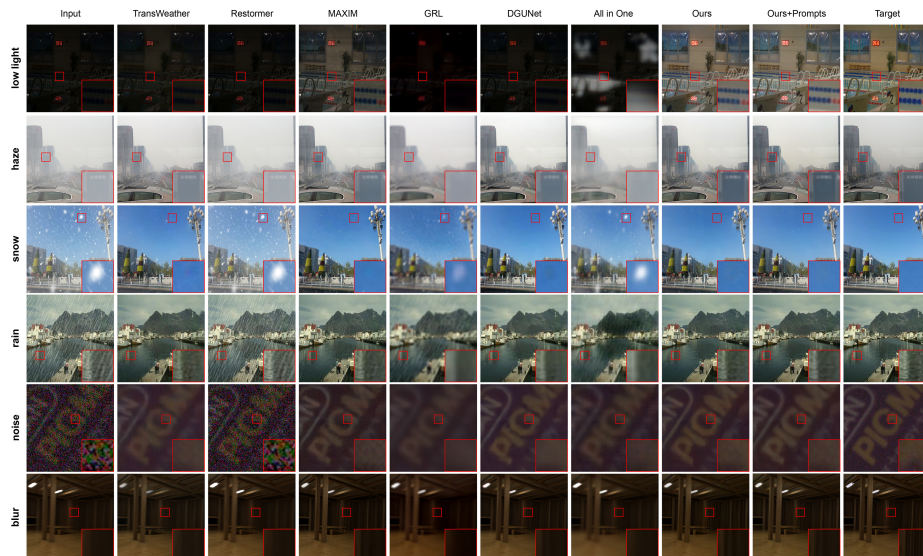


Fig. 6: Visual comparison with SOTA image restoration algorithms in different image restoration tasks.

be performed on the image by themselves. In addition, we found that Restormer can remove complex compound degenerates from an image by stacking textual prompts in the real world (see Figure 9). To the best of our knowledge, this is what previous image restoration methods fail to do.

Furthermore, we also show the performance of Restormer on SIDD based on different textual prompts in Figure 5. It can be observed that Restormer based on different prompts also exhibits similar performance on SIDD as on the RealBlur-R dataset. Restormer also strictly follows the textual prompts to perform the appropriate image restoration tasks. Moreover, by stacking text prompts Restormer also removes the complex degradation of noise and low-light composites. This suggests that the success of Restormer based on textual prompts is no accident. We hope that this finding will be useful for composite degraded restoration tasks.

3.4 Overall Loss

Restormer uses smooth L1-loss and perceptual loss in TransWeather to restore the pixels and content of the input image. The total loss is formulated as follows:

$$L_{total} = L_{smoothL_1} + \lambda L_{perceptual}, \quad (3)$$

where $\lambda = 0.04$ is used to control the contribution of perceptual loss in the total loss of Restormer.

4 Experiments

We evaluated Restormer on six different image restoration tasks: deraining, desnowing, defogging, deblurring, denoising, and low-light image enhancement. Ablation

Method	deraining		desnowing		defogging		denoising		low-light enhancement		deblurring				Average	
	rain1400		CSD		SOTS		SIDD		LOL		GoPro		RealBlur-R			
	PSNR ↑	SSIM(%) ↑	PSNR ↑	SSIM(%) ↑	PSNR ↑	SSIM(%) ↑	PSNR ↑	SSIM(%) ↑	PSNR ↑	SSIM(%) ↑	PSNR ↑	SSIM(%) ↑	PSNR ↑	SSIM(%) ↑	PSNR ↑	SSIM(%) ↑
GRL [36]	20.56	79.71	20.45	80.01	21.71	84.97	33.81	93.53	7.09	3.82	18.50	77.94	27.58	49.15	21.42	67.01
Uformer [61]	31.74	95.49	27.46	92.61	29.85	97.82	38.35	96.26	8.50	26.84	25.89	91.38	37.13	95.86	28.41	85.18
DFCNet [39]	33.05	96.52	28.81	92.28	31.04	96.22	39.61	97.04	13.04	55.37	30.06	94.04	37.74	96.36	30.47	89.69
MPRNet [7]	33.47	96.59	28.03	92.57	30.96	97.40	38.94	96.77	15.78	71.15	28.39	94.10	37.50	96.75	30.43	92.18
Restormer [8]	24.38	87.60	14.30	72.67	15.94	82.92	25.30	65.35	7.79	19.79	26.22	87.15	34.42	96.83	21.19	73.18
MAXIM [5]	32.63	96.80	27.81	92.20	32.20	98.14	27.70	95.95	13.48	78.33	25.78	93.39	32.52	91.87	27.44	92.38
NAFNet [6]	32.87	97.32	28.31	92.65	32.34	96.74	29.89	96.18	21.57	89.37	25.58	93.46	32.91	95.18	29.06	94.41
TransWeather [56]	34.27	96.25	29.38	92.22	32.96	96.55	36.14	95.69	15.72	62.90	29.03	93.78	39.00	93.06	30.92	90.06
SYENet [18]	30.02	89.11	22.55	87.35	26.37	95.66	33.19	91.03	17.64	81.57	26.78	93.30	35.90	94.92	27.49	90.42
All in One [34]	24.63	83.67	18.40	72.28	18.14	76.86	35.10	87.30	11.24	32.10	24.18	85.88	26.94	85.57	22.66	74.80
Ours	33.61	96.33	29.93	92.71	34.19	98.21	37.74	96.36	21.60	89.86	30.12	94.85	41.08	95.20	32.09	94.78
Ours+Prompts	34.21	96.70	30.28	93.09	34.46	98.25	37.75	96.36	21.44	90.53	30.92	95.48	43.10	97.55	33.16	95.42

Table 1: Quantitative Comparison with SOTA unified image restoration methods and all-in-one image restoration methods.

study, more specific experimental details, and more comprehensive results can be found in the **Appendix**.

4.1 Experimental Setup

Datasets and metrics. We employ PSNR and SSIM (%) metrics to evaluate Restorer. We unify several datasets as "mixed training set" of image restoration tasks for Restorer training and validate Restorer performance with official test sets, including CSD [8], rain1400 [16], OTS [33], SIDD [1], LOL [62], GoPro [40], and RealBlur-R [50]. See the Appendix A for details on the setting of the dataset.

Implementation details. Restorer employs the PyTorch framework. Restorer is trained for 250 epochs with a batch size of 26. The rest of the settings followed TransWeather. The architecture configuration and model complexity for Restorer can be found in the Appendix B.

4.2 Main Results

Comparison with unified image restoration methods. In this section, we compare Restorer with current SOTA unified image restoration methods [6, 18, 34, 36, 39, 55, 56, 61, 68, 70]. All algorithms are trained uniformly on mixed training sets according to the official settings and tested under the official test set for each image restoration task. We report numerical results for Restorer with above baselines on multiple image restoration tasks in Table 4. Compared to current SOTA methods, our method exhibits SOTA or competitive PSNR and SSIM results on multiple image restoration tasks. The visualization in Figure 6 shows that compared to other baselines our method can be successfully applied to multiple image restoration tasks, closer to the ground truth while maintaining clarity.

Deraining. We compare Restorer to expert networks designed for deraining tasks. We cite results in [9] where these networks are trained and tested on rain1400. The improvements of our Restorer method in image deraining are shown in Table 2a. In Figure 7, both our method and most baselines obtain high-quality restored images in deraining. Restorer restores more fine detail of the original image compared to the deraining baselines (see green-boxed area).

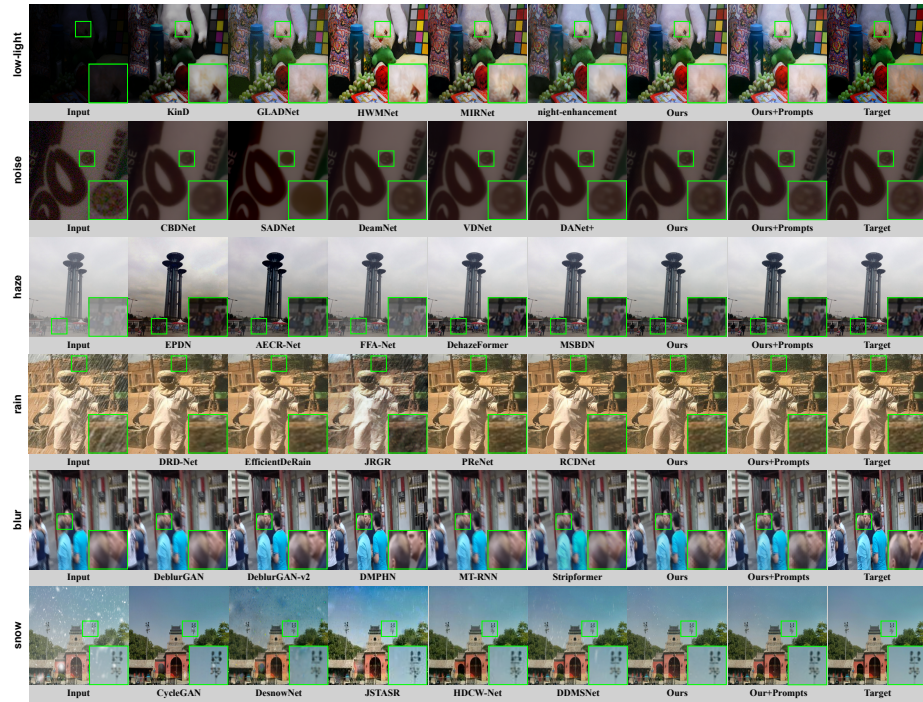


Fig. 7: Qualitative comparison results of Restorer with expert networks on individual image restoration tasks.

Desnowing. Table 2c shows the numerical comparison results between Restorer and desnowing expert networks trained on CSD. It can be seen that Restorer’s PSNR and SSIM on the CSD dataset are 0.87 dB PSNR and 1.71% SSIM higher than the previous SOTA method. Additionally, the Restorer with text prompts has a higher gain of 1.18dB PSNR and 2.09% SSIM. As shown in Figure 7, Restorer successfully removes snow particles from the input image and does not suffer from the artifact issue in HDCW-Net [8] compared to the desnowing baselines.

Defogging. Restorer is compared with defogging networks trained on the OTS dataset. We mainly cite the results from [9]. Although Restorer is not achieving SOTA results on SOTS, its 34.19dB PSNR and 98.21% SSIM metrics in Table 2b are still competitive. Figure 7 shows that Restorer achieves effective defogging while restoring the global hue of the input image. Thus, the visual results of Restorer restored images are more satisfactory.

Deblurring. To validate the performance of Restorer on deblurring, we compare it with methods trained on GoPro and RealBlur-R, respectively. Compared to these expert networks, Our SSIM metric on the GoPro is highly competitive. See the Appendix E for comparison results on the RealBlur-R dataset. Figure 7 shows a visual comparison of the evaluated models on GoPro. It can be observed that Restorer shows satisfactory results on the deblurring task.

Method	PSNR	SSIM (%)
JORDER [64]	31.28	92.00
PReNet [49]	31.88	93.00
DRD-Net [11]	29.65	88.00
MSPFN [26]	29.24	88.00
EfficientDeRain [21]	32.30	92.72
JRGR [65]	31.18	91.00
RCDNet [59]	33.04	94.72
Ours	33.61	96.33
Ours+Prompts	34.21	96.70

(a) **Deraining.** rain1400 draining results.

Method	PSNR	SSIM (%)
EPDN [46]	23.82	87.00
PFDN [13]	31.45	97.00
KDDN [23]	29.16	94.00
MSBDN [12]	33.79	98.00
FFA-Net [45]	34.98	99.00
AECRNet [63]	35.61	98.00
DehazeFormer [52]	34.29	98.30
Ours	34.19	98.21
Ours+Prompts	34.46	98.25

(b) **Defogging.** SOTS defogging results.

Method	PSNR	SSIM (%)
DesnowNet [38]	20.13	81.00
CycleGAN [76]	20.98	80.00
JSTASR [7]	27.96	88.00
DDMSNet [73]	27.24	82.00
HDCW-Net [8]	29.06	91.00
DesnowGAN [25]	28.63	90.00
Ours	29.93	92.71
Ours+Prompts	30.28	93.09

(c) **Desnowing.** CSD desnowing results.

Method	PSNR	SSIM (%)
GLADNet [60]	19.71	70.30
EnlightenGAN [27]	17.48	65.70
KinD [75]	20.37	80.40
MIRNet [69]	24.14	83.00
night-enhancement [28]	21.52	76.30
HWMNet [15]	24.24	85.20
Ours	21.60	89.86
Ours+Prompts	21.44	90.53

(d) **Low-light Enhancement.** LOL low-light enhancement results.

Method	PSNR	SSIM (%)
CBDNet [22]	30.78	80.10
AINDNet [30]	39.08	95.40
VDN [66]	39.28	95.60
SADNet [4]	39.46	95.70
DANet+ [67]	39.47	95.70
DeamNet [48]	39.47	95.70
Ours	37.74	96.36
Ours+Prompts	37.75	96.36

(e) **Denoising.** SIDD denoising results.

Method	PSNR	SSIM (%)
DeblurGAN [31]	28.70	85.80
DeblurGAN-v2 [32]	29.55	93.40
DBGAN [74]	31.10	94.20
MT-RNN [41]	31.15	94.50
DMPHN [71]	31.20	94.00
Stripformer [54]	33.08	96.20
Ours	30.12	94.85
Ours+Prompts	30.92	95.48

(f) **Deblurring.** GoPro deblurring results.

Table 2: Quantitative comparison of Restorer with several different types of image restoration expert networks.

Denoising. As shown in Table 2e, our method achieves the best SSIM values on the denoising task compared to the expert network trained on SIDD alone. This indicates that our approach is competitive. Compared to baselines, Restorer effectively removes real noise and produces sharper restored results (see Figure 7).

Low-light Enhancement. We report the comparison results of Restorer with the low-light enhancement expert networks trained on the LOL dataset in Table 2d. Our PSNR achieves competitive results and our SSIM is increased by 4.66% compared to the previous SOTA method. And Restorer based on textual prompts even achieves 90.53% SSIM. In Figure 7, while the baselines all achieve low-light enhancement well, they suffer from a degree of overexposure and chromatic aberration (see green-boxed area). In comparison, Restorer restores images closer to the target.

4.3 Real-world Tests

In this section, we test Restorer based on textual prompts performance on real-world datasets to verify that it can be applied in real scenarios. Since Restorer’s performance on image restoration tasks such as denoising, deblurring, and low-light enhancement are all verified on real-world datasets, we only need to select



Fig. 8: Sample qualitative image restoration results on the real-world rain, haze, and snow degradations.

real-world image restoration tasks for severe weather to evaluate. Figure 8 shows the comparison results of our algorithm with several SOTA algorithms for image restoration on real datasets. Compared to each baseline, Our method performs more robustly on real-world datasets. We also provide visual comparison results between Restormer and the baselines on real-world severe weather image restoration in Appendix F.

Setting	Module			Metric
	AAA	3D-DCFFN	TQ	PSNR/SSIM
Baseline				14.18 / 0.705
s1	✓			25.44 / 0.902
s2	✓	✓		28.26 / 0.919
s3	✓	✓	✓	29.93 / 0.927

Table 3: Ablation of Core Designs. TQ represents Task Queries.

4.4 Ablation Study

We conduct extensive ablation studies to validate the contribution of AAA, 3D-DCFFN, and learnable task queries to Restormer. The U-Net with Restormer’s four-stage encoder-decoder framework is used as the baseline for our ablation study. Then we gradually add AAA, 3D-DCFFN, and learnable task queries to the baseline. Table 6 shows that each design of this work contributes to the performance of Restormer. See Appendix D for more ablation results.

5 Conclusion

In this work, we propose Restormer to handle multiple image restoration tasks. With this aim, we introduce an all-axis attention module that has complementary advantages of spatial attention and channel attention. Furthermore, the proposed 3D-DCFFN preserves the fine details in the image in both spatial and channel dimensions. Meanwhile, Restormer based on textual prompts solves the task confusion issue and introduces an interaction element. Extensive experiments have shown that Restormer has the potential to serve as the backbone of real-world image restoration applications.

Task	Dataset	#Train	#Test	Test Dubname
Desnowing	CSD [8]	5000	2000	CSD
Deraining	rain1400 [16]	5000	1400	rain1400
Dehazing	OTS [33]	5000	500	SOTS
Denoising	SIDD [1]	5000	1280	SIDD
Deblurring	GoPro [40]	2103	1111	GoPro
	RealBlur-R [50]	3758	980	RealBlur-R
Enhancement	LOL [62]	485	15	LOL

Table 4: Dataset configuration on six image restoration tasks.

A Datasets

To train Restorer which can be applied to multiple image restoration tasks, our mixed training set is selected from several standard image restoration datasets including CSD [8], rain1400 [16], OTS [33], SIDD [1], LOL [62], GoPro [40], and RealBlur-R [50]. For the desnowing task, we randomly selected 5K images from the CSD training set containing 10K synthetic snow images for the mixed training set. In the testing phase, we use the official CSD test set for testing. Regarding the deraining task, we randomly selected 5000 images from the rain1400 training set containing 12600 synthetic rainfall images to the mixed training set and validated Restorer with the official rain1400 test set. For the training of Restorer defogging, the mixed training set has 5000 images randomly selected from the OTS dataset according to the settings of Chen et al. [9]. We applied SOTS for the defogging test. Regarding denoising, the mixed training set consists of 5K images randomly selected from a SIDD containing 30K real noisy images. For the testing phase, we chose the official SIDD test set. For the low-light enhancement task, we select the LOL dataset containing 485 training images and 15 test images for training and testing. Regarding the deblurring task, the mixed training set includes 2103 GoPro and 3758 RealBlur-R training images. Regarding the deblurring tests, we used the official test sets of GoPro and RealBlur-R respectively. Detailed dataset settings are shown in Table 4.

B Complexity

The detailed specifications of the Restorer architecture configuration are shown in Table 5. We have provided the input shapes and output shapes for each stage of the Restorer encoder for better understanding. We reduce the computational overhead of AAA module by adjusting the spatial dimension p and the channel dimension d of the stereo token embedding at each stage. Also for this purpose, we unify the embedding dimension D of each stage to 512 dimensions. See Table 6 for a comparison of performance and complexity between our method and competing methods. Moreover, we show the complexity of each component in Restorer in Table 7. It can be noticed that our AAA module and 3D-DCFFN do not lead to a huge amount of computation.

Architecture			
Stage	Input shape	Output Shape	Layers
Stage1	$256^2 \times 3$	$128^2 \times 128$	$N_1 = 3, p = 16,$ $d = 16, D = 512, H = 2$
Stage2	$128^2 \times 128$	$64^2 \times 128$	$N_2 = 4, p = 8,$ $d = 16, D = 512, H = 2$
Stage3	$64^2 \times 128$	$32^2 \times 256$	$N_3 = 6, p = 4,$ $d = 32, D = 512, H = 4$
Stage4	$32^2 \times 256$	$16^2 \times 512$	$N_4 = 3, p = 4,$ $d = 16, D = 512, H = 8$

Table 5: Detailed architectural configurations for the different stages of Restorer.

Task	Dataset	Model	PSNR	FLOPs
Denoise	SIDDD [1]	Restormer [68]	25.30	141G
		MAXIM [55]	27.70	216G
		Ours	37.74	147G
		Ours+Prompts	37.75	147G
Deblur	GoPro [40]	Restormer [68]	26.22	141G
		MAXIM [55]	25.78	216G
		Ours	30.12	147G
		Ours+Prompts	30.92	147G
Deblur	RealBlur-R [50]	Restormer [68]	34.42	141G
		MAXIM [55]	32.52	216G
		Ours	41.68	147G
		Ours+Prompts	43.10	147G
Derain	rain1400 [16]	Restormer [68]	24.38	141G
		MAXIM [55]	32.63	216G
		Ours	33.61	147G
		Ours+Prompts	34.21	147G
Dehaze	SOTS	Restormer [68]	15.94	141G
		MAXIM [55]	32.20	216G
		Ours	34.19	147G
		Ours+Prompts	34.46	147G
Enhance	LOL [62]	Restormer [68]	7.79	141G
		MAXIM [55]	13.48	216G
		Ours	21.60	147G
		Ours+Prompts	21.44	147G

Table 6: Model performance *vs.* complexity comparison of our model with SOTA baselines.

Setting	Module			FLOPs
	AAA	3D-DCFFN	TQ	
Baseline				147G
s1		✓	✓	121G
s2	✓		✓	144G
s3	✓	✓		147G

Table 7: Ablation of Core Designs. TQ represents Task Queries.

C Experimental Details

Restorer mainly follows the [56] settings. Apart from the training settings described in the main text, Restorer uses 256-resolution images as input and performs normalization operations on the input data. In addition, for training after 60 epochs, the learning rate decays by half every 50 epochs. We implemented Restorer training with two NVIDIA RTX 3090.

D Ablation Study

Effectiveness of AAA. To further validate the effectiveness of AAA, we also test the performance of Restorer paired with different attention mechanisms. Table 8d shows that AAA is more suitable for Restorer to handle multiple image restoration tasks at the same time than other attention mechanisms.

Effectiveness of 3D-DCFFN. We compare the results of different feedforward networks on Restorer. Table 8c shows that our 3D-DCFFN better improves the quality of restored images compared to other feedforward network backbones. Therefore, 3D-DCFFN is the key for Restorer to get high-quality restored images.

AAA Connection. We removed the connection between the AAA modules. As shown in Table 8a, after removing the connection between the AAA modules, Restorer’s effectiveness on the desnowing task decreases to some extent. This suggests that the connections between the AAA modules we designed to enhance Restorer’s multiscale play a role.

Encoder Module and Decoder Module Structure. Regarding the ablation design of the structure of Restorer’s encoder and decoder modules, we choose Restormer’s [68] Transformer block to replace them respectively. In Table 8a, each of these ablation designs resulted in a decrease in the Restorer metric. One possible reason for this is that convolution inherently has local modeling advantages that Transformer does not have. This facilitates Restorer’s restored image to retain fine details in the original image.

Negative Affinity Matrices. We test the effectiveness of negative affinity matrices coupled with learnable task queries in all-axis attention in this section. We compare the negative affinity matrices with two variants, the vanilla affinity matrices, and the projection affinity matrices. With Table 8b we observe that the negative affinity matrices are more favorable to Restorer. We believe this is because the negative affinity matrices explicitly model the relationship between the learnable task queries and the image restoration tasks. Compared to other types of affinity matrices, this explicit modeling of negative affinity matrices provides an explicit goal for learnable task queries, i.e., fitting the degradation features of the corresponding image restoration task. As a result, Restorer with negative affinity matrices can achieve more accurate image restoration.

Method	Metric	
	PSNR	SSIM
w/o AAA connection	28.75	0.924
w/ Restormer encoder module	28.51	0.923
w/ Restormer decoder module	28.26	0.920

(a) Ablation results for AAA connections, encoder modules, and decoder modules in Restorer.

Method	Metric	
	PSNR	SSIM
w/ vanilla affinity matrices	29.47	0.922
w/ projection affinity matrices	29.19	0.924
w/ negative affinity matrices	29.93	0.927

(b) Effectiveness of negative affinity matrices in all-axis attention.

Method	Metric	
	PSNR	SSIM (%)
w/ vanilla FFN	28.14	92.07
w/ DCFFN	28.65	92.38
w/ 3D-DCFFN	29.93	92.71

(c) Effects of 3D-DCFFN.

Method	Metric	
	PSNR	SSIM (%)
w/ spatial attention	25.61	90.33
w/ channel attention	24.85	89.72
w/ OSA	27.92	92.26
w/ AAA	29.93	92.71

(d) Effectiveness of AAA.

Table 8: Ablation results for each component of Restorer. We report ablation results using desnowing experiments on CSD.

E More Experiments

In this section, we provide quantitative comparisons and qualitative comparison results between Restorer and the deblurring expert networks trained and tested on RealBlur-R alone. We choose multiple current SOTA deblurring baselines for comparison. Figure 9 and Table 9 demonstrate the results of qualitative and quantitative comparisons, respectively.

Method	Venue	Metric	
		PSNR	SSIM
DeblurGAN [31]	CVPR	33.79	0.9030
DeblurGAN-v2 [32]	ICCV	35.26	0.9440
SRN [53]	CVPR	35.66	0.9470
DBGAN [74]	CVPR	33.78	0.9090
MT-RNN [41]	ECCV	35.79	0.9510
DMPHN [71]	ECCV	35.70	0.9480
MIMO-UNet+ [10]	ICCV	35.54	0.9470
Stripformer [54]	ECCV	39.84	<u>0.9740</u>
MSSNet [29]	ICCV	39.76	0.9720
Ours	-	<u>41.68</u>	0.9520
Ours+Prompts	-	43.10	0.9755

Table 9: Quantitative comparison results of Restorer with multiple deblurring baselines on RealBlur-R.

Quantitative Results. As shown in Table 9, our Restorer achieves state-of-the-art performance for the deblurring task on RealBlur-R. Compared to the current SOTA deblurring baselines, Restorer offers a large improvement over

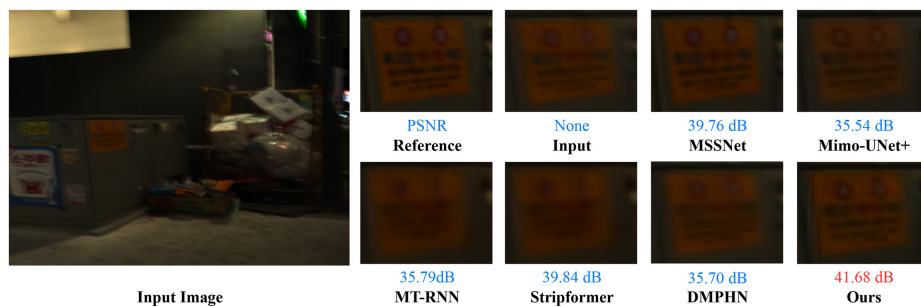


Fig. 9: Visual comparison results between Restorer and SOTA deblurring baselines on RealBlur-R.

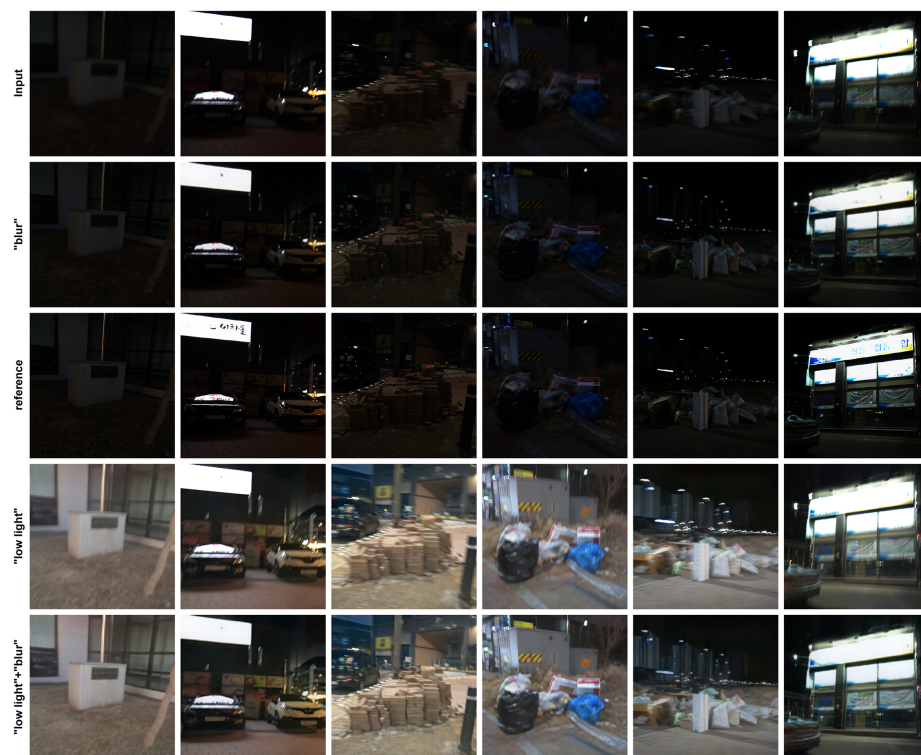


Fig. 10: Restorer's image restoration results at different textual prompts on RealBlur-R.

PSNR. Specifically, Restorer improved by 1.92 dB compared to MSSNet [29] and 1.84 dB compared to Stripformer [54]. Meanwhile, Restorer based on textual prompts achieves state-of-the-art performance as evaluated by PSNR and SSIM metrics.

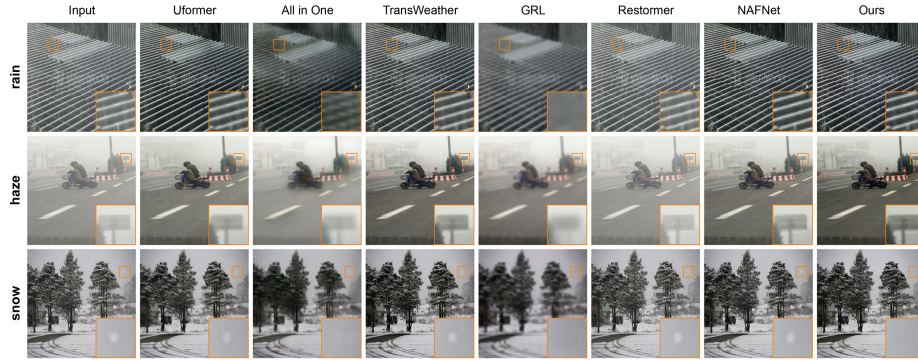


Fig. 11: Qualitative comparison results between Restormer and baselines in the real world.

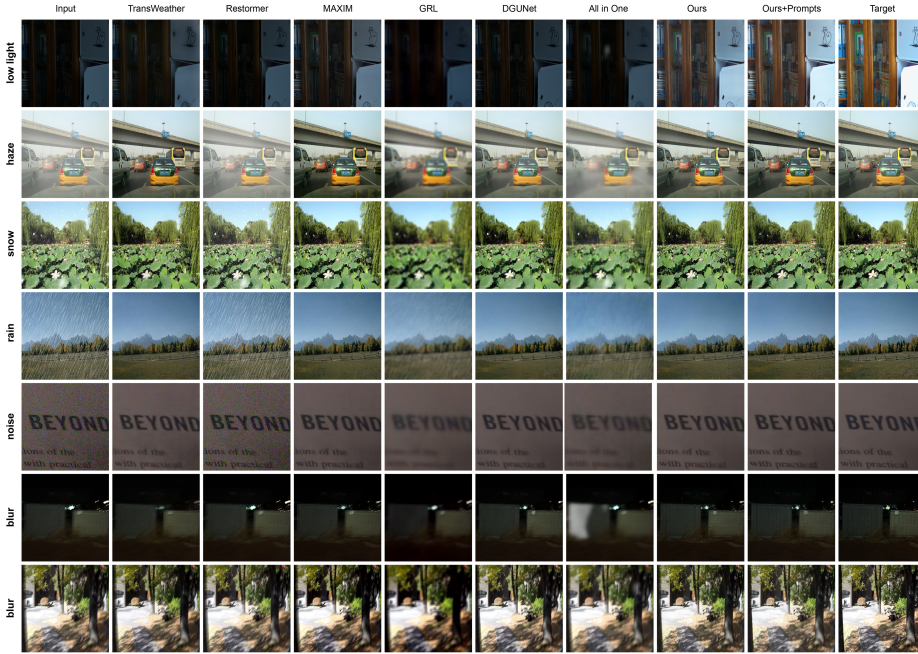


Fig. 12: Qualitative comparison results between Restormer and SOTA unified image restoration algorithms and all-in-one image restoration algorithms.

Qualitative Results. Figure 9 shows the qualitative comparison results between Restormer and the current SOTA deblurring baselines on RealBlur-R. It can be observed that our model restores the blurred text well. This may be attributed to the fact that the use of the AAA module at each stage allows the module to globally aggregate repeating patterns at different scales.

F Real-world Comparisons

In this section, we show the visual comparison results between the Restorer and baselines under different degradation conditions in the real world. Figure 11 shows that Restorer better removes degradation from the image and produces sharper results than many excellent baselines. This shows that Restorer is robust enough to degradations in real scenarios.

G Restorer Based on Textual Prompts

In this section, we provide more visual results of Restorer employing different textual prompts for the degraded image. We also demonstrate the effectiveness of Restorer’s restoration of complex composite degraded images by making it stack several textual prompts.

As shown in Figure 10, Restorer successfully performs different image restoration tasks on the RealBlur-R dataset following different textual prompts. Meanwhile, by stacking textual prompts, Restorer successfully restores input images with complex composite degradation.

H More Visual Results

Comparison with Unified Image Restoration Algorithms. We show the visual comparison results of Restorer with several SOTA unified image restoration algorithms and all-in-one image restoration algorithms in Figure 12. Compared to these excellent baselines, our method successfully removed various types of degradation and obtained pleasing visual results.

Desnowing. As shown in Figure 13, our method successfully removes snow particles of different sizes from the input image without artifacts and chromatic aberration problems compared to multiple SOTA desnowing expert networks that were individually trained and tested on CSD dataset.

In Figure 14, most of the baselines fail to remove the snow particles from the degraded image and cause severe impairments to the restored image. In contrast, with the text "snow" prompt, Restorer successfully removed the snow particles in the image and obtained a pleasant restored result.

Deraining. Figure 15 shows the visual comparison results between Restorer and the current state-of-the-art deraining expert networks on rain1400. It can be observed that our method effectively removes the rain from the input image and successfully obtains a high-quality restored image.

We compare the performance of Restorer based on textual prompts and expert networks on deraining in Figure 16. Compared to these excellent baselines, Restorer based on textual prompts successfully removed rain and had no problems with artifacts.

Defogging. We provide a defogging visual comparison in Figure 17. Restorer restored more satisfactory results in the defogging task than other methods.

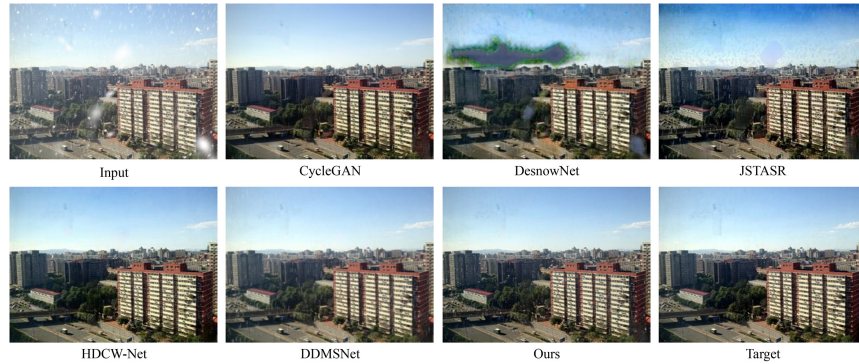


Fig. 13: Visual comparison results between Restorer and SOTA desnowing baselines on CSD dataset.

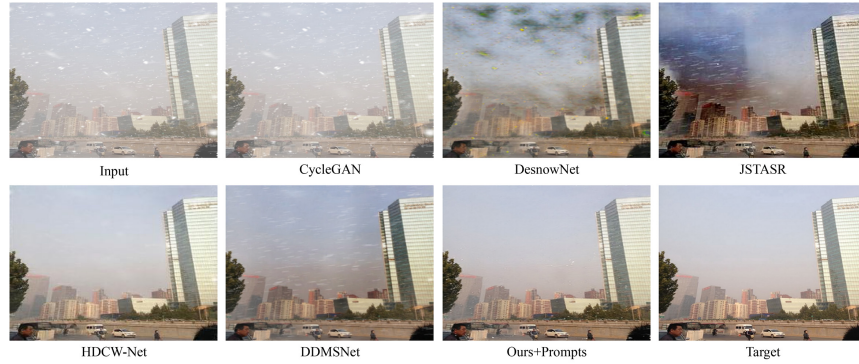


Fig. 14: Visual comparison results between Restorer based on textual prompts and SOTA desnowing baselines on CSD dataset.

On the qualitative comparison of defogging in Fig 18, although all the comparison algorithms successfully remove the degradation, EPDN [46], AECR-Net [63], and FFA-Net [45] produce severe chromatic aberration affecting the quality of the restored images. On the other hand, DehazeFormer [52] and MS-BDN [12] have some fog residuals in the house area. Compared with them, Restorer based on textual prompts has a more obvious defogging effect and more satisfactory image restoration results.

Deblurring. The visualizations on GoPro [40] and RealBlur-R [50] are shown in Figure 19 and Figure 21, respectively, and our model achieves competitive results on both real-world deblurring benchmarks.

Furthermore, Restorer based on textual prompts also successfully removes degradation on GoPro and RealBlur-R in Figure 20 and Figure 22. This proves that both Restorer and Restorer based on textual prompts are robust enough for blurring.

Denosing. The qualitative comparison results of the denoising task for the SIDD dataset are shown in Figure 23. Both our method and the comparison

baselines successfully remove the noise from the input image. But Restorer provides clearer restored results than many baselines.

In the denoising results in Figure 24, Restorer based on textual prompts successfully removes the noise degradation and restores fine details in the image. We attribute this to the success of convolution in local modeling in 3D-DCFFN, encoder, and decoder structures in Restorer.

Low-light Enhancement. We show qualitative comparison results of Restorer with current state-of-the-art low-light enhancement algorithms in Figure 25. It can be observed that our method successfully achieves low-light enhancement and obtains pleasing visual effects that are closer to the ground truth.

We can also observe in Figure 26 that Restorer based on low-light textual prompts achieves a more obvious light enhancement effect.

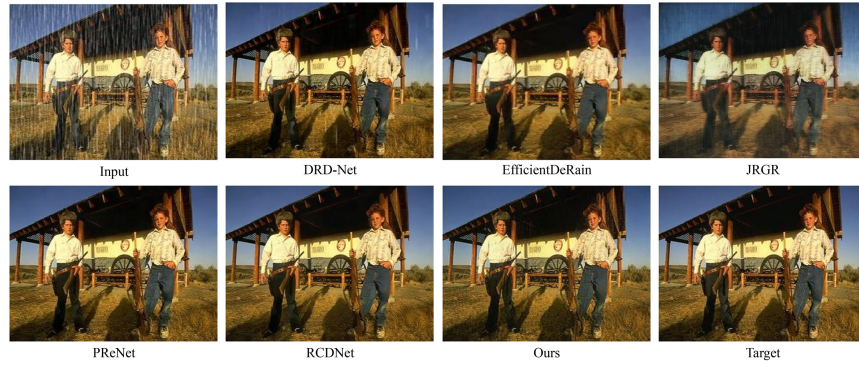


Fig. 15: Visual comparison results between Restorer and SOTA deraining baselines on rain1400.

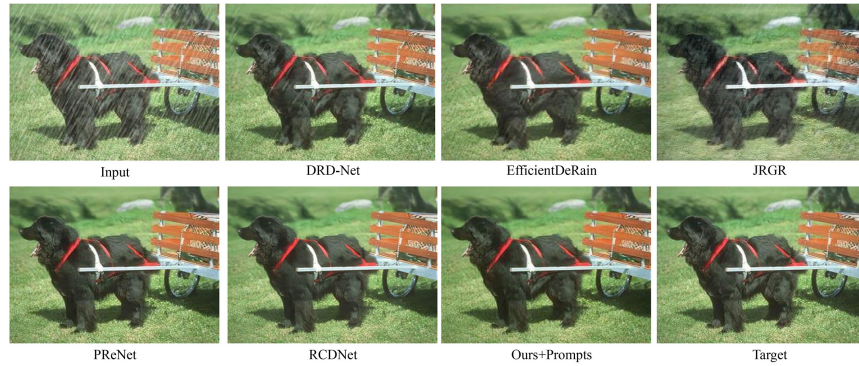


Fig. 16: Visual comparison results between Restorer based on textual prompts and SOTA deraining baselines on rain1400.

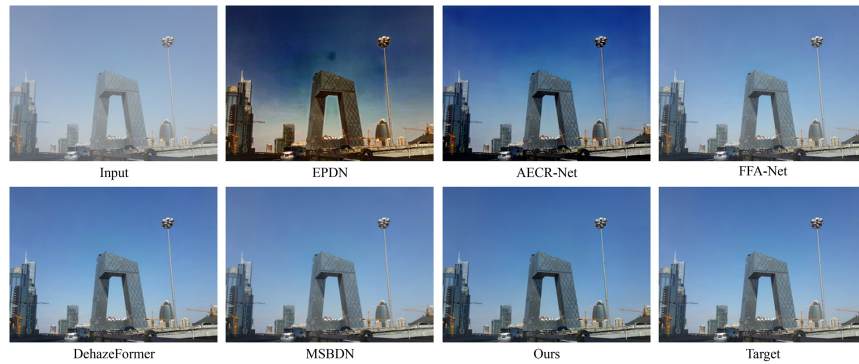


Fig. 17: Visual comparison results between Restorer and SOTA defogging baselines on SOTS.



Fig. 18: Visual comparison results between Restorer based on textual prompts and SOTA defogging baselines on SOTS.

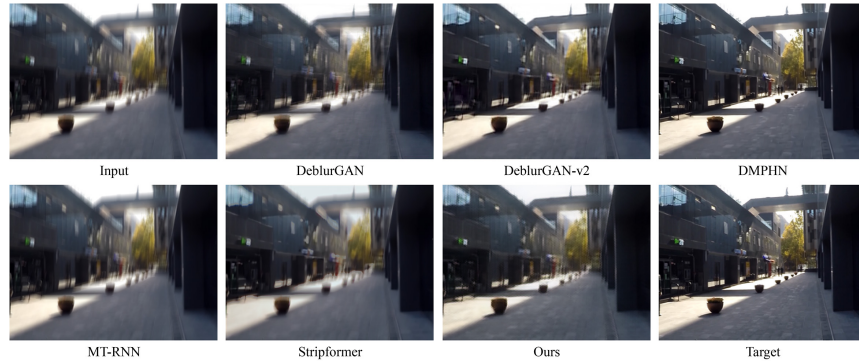


Fig. 19: Visual comparison results between Restorer and SOTA deblurring baselines on GoPro.

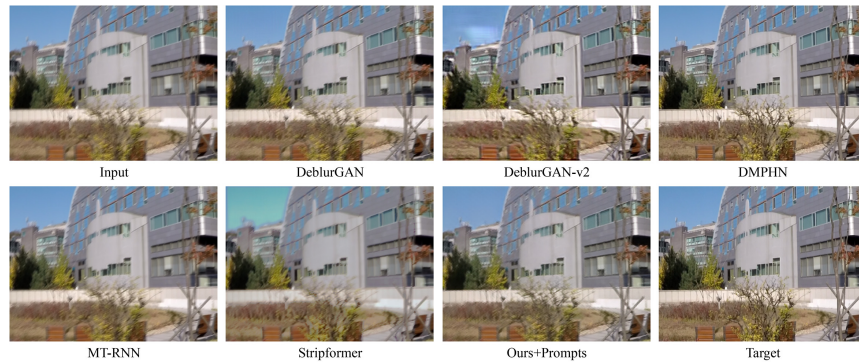


Fig. 20: Visual comparison results between Restorer based on textual prompts and SOTA deblurring baselines on GoPro.



Fig. 21: Visual comparison results between Restorer and SOTA deblurring baselines on RealBlur-R.

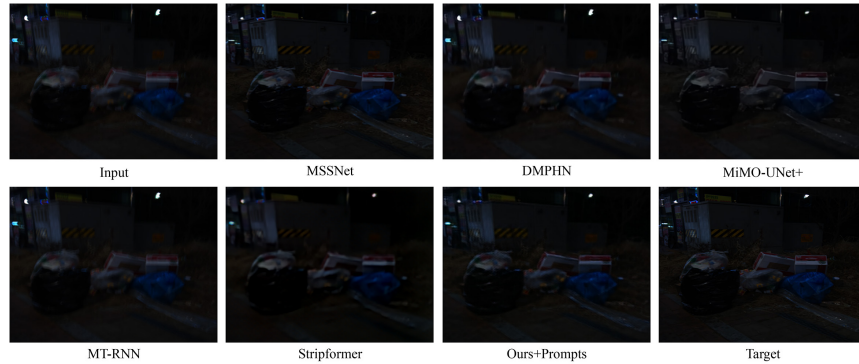


Fig. 22: Visual comparison results between Restorer based on textual prompts and deblurring baselines on RealBlur-R.

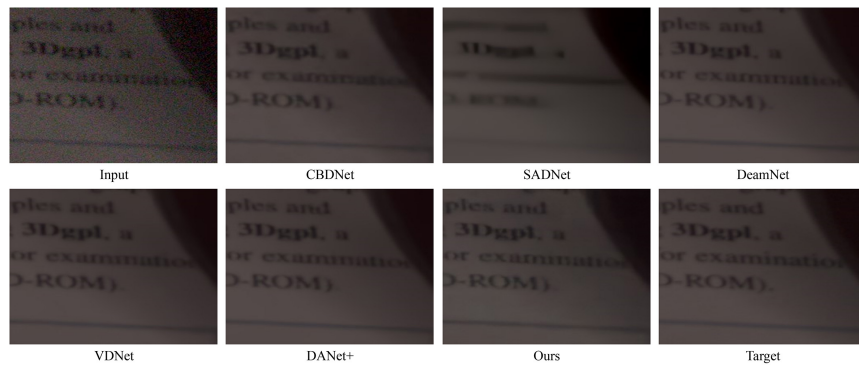


Fig. 23: Visual comparison results between Restorer and SOTA denoising baselines on SSIM.

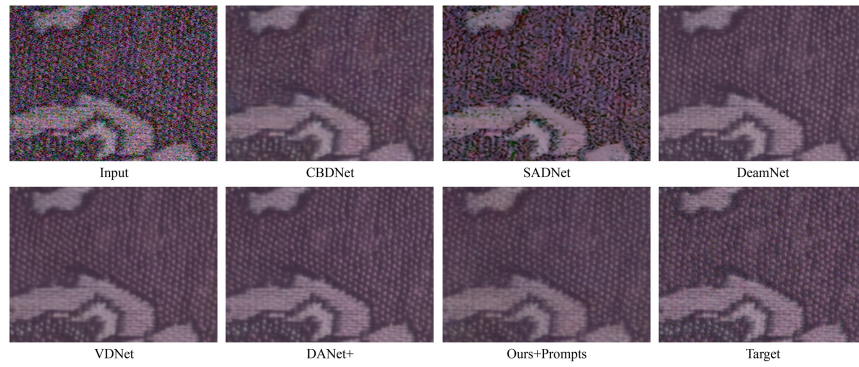


Fig. 24: Visual comparison results between Restorer based on textual prompts and SOTA denoising baselines on SSIM.

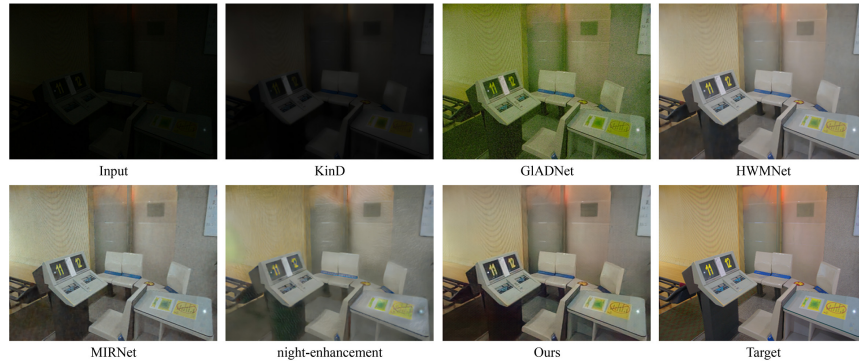


Fig. 25: Visual comparison results between Restorer and SOTA low-light enhancement baselines on LOL dataset.



Fig. 26: Visual comparison between Restorer based on textual prompts and low-light enhancement baselines on LOL.

References

1. Abdelhamed, A., Lin, S., Brown, M.S.: A high-quality denoising dataset for smartphone cameras. In: Proceedings of the IEEE conference on computer vision and pattern recognition. pp. 1692–1700 (2018) [11](#), [15](#), [16](#)
2. Ba, J.L., Kiros, J.R., Hinton, G.E.: Layer normalization. arXiv preprint arXiv:1607.06450 (2016) [7](#)
3. Carion, N., Massa, F., Synnaeve, G., Usunier, N., Kirillov, A., Zagoruyko, S.: End-to-end object detection with transformers. In: European conference on computer vision. pp. 213–229. Springer (2020) [5](#)
4. Chang, M., Li, Q., Feng, H., Xu, Z.: Spatial-adaptive network for single image denoising. In: Computer Vision–ECCV 2020: 16th European Conference, Glasgow, UK, August 23–28, 2020, Proceedings, Part XXX 16. pp. 171–187. Springer (2020) [13](#)
5. Chen, H., Wang, Y., Guo, T., Xu, C., Deng, Y., Liu, Z., Ma, S., Xu, C., Xu, C., Gao, W.: Pre-trained image processing transformer. In: Proceedings of the IEEE/CVF conference on computer vision and pattern recognition. pp. 12299–12310 (2021) [7](#)
6. Chen, L., Chu, X., Zhang, X., Sun, J.: Simple baselines for image restoration. In: European Conference on Computer Vision. pp. 17–33. Springer (2022) [5](#), [11](#)
7. Chen, W.T., Fang, H.Y., Ding, J.J., Tsai, C.C., Kuo, S.Y.: Jstasr: Joint size and transparency-aware snow removal algorithm based on modified partial convolution and veiling effect removal. In: European Conference on Computer Vision. pp. 754–770. Springer (2020) [13](#)
8. Chen, W.T., Fang, H.Y., Hsieh, C.L., Tsai, C.C., Chen, I., Ding, J.J., Kuo, S.Y., et al.: All snow removed: Single image desnowing algorithm using hierarchical dual-tree complex wavelet representation and contradict channel loss. In: Proceedings of the IEEE/CVF International Conference on Computer Vision. pp. 4196–4205 (2021) [2](#), [11](#), [12](#), [13](#), [15](#)
9. Chen, W.T., Huang, Z.K., Tsai, C.C., Yang, H.H., Ding, J.J., Kuo, S.Y.: Learning multiple adverse weather removal via two-stage knowledge learning and multi-contrastive regularization: Toward a unified model. In: Proceedings of the IEEE/CVF Conference on Computer Vision and Pattern Recognition. pp. 17653–17662 (2022) [2](#), [5](#), [11](#), [12](#), [15](#)
10. Cho, S.J., Ji, S.W., Hong, J.P., Jung, S.W., Ko, S.J.: Rethinking coarse-to-fine approach in single image deblurring. In: Proceedings of the IEEE/CVF international conference on computer vision. pp. 4641–4650 (2021) [18](#)
11. Deng, S., Wei, M., Wang, J., Feng, Y., Liang, L., Xie, H., Wang, F.L., Wang, M.: Detail-recovery image deraining via context aggregation networks. In: Proceedings of the IEEE/CVF conference on computer vision and pattern recognition. pp. 14560–14569 (2020) [13](#)
12. Dong, H., Pan, J., Xiang, L., Hu, Z., Zhang, X., Wang, F., Yang, M.H.: Multi-scale boosted dehazing network with dense feature fusion. In: Proceedings of the IEEE/CVF conference on computer vision and pattern recognition. pp. 2157–2167 (2020) [2](#), [13](#), [22](#)
13. Dong, J., Pan, J.: Physics-based feature dehazing networks. In: Computer Vision–ECCV 2020: 16th European Conference, Glasgow, UK, August 23–28, 2020, Proceedings, Part XXX 16. pp. 188–204. Springer (2020) [13](#)
14. Dosovitskiy, A., Beyer, L., Kolesnikov, A., Weissenborn, D., Zhai, X., Unterthiner, T., Dehghani, M., Minderer, M., Heigold, G., Gelly, S., et al.: An image is worth 16x16 words: Transformers for image recognition at scale. arXiv preprint arXiv:2010.11929 (2020) [7](#)

15. Fan, C.M., Liu, T.J., Liu, K.H.: Half wavelet attention on m-net+ for low-light image enhancement. In: 2022 IEEE International Conference on Image Processing (ICIP). pp. 3878–3882. IEEE (2022) [2](#), [13](#)
16. Fu, X., Huang, J., Zeng, D., Huang, Y., Ding, X., Paisley, J.: Removing rain from single images via a deep detail network. In: Proceedings of the IEEE conference on computer vision and pattern recognition. pp. 3855–3863 (2017) [11](#), [15](#), [16](#)
17. Fu, X., Qi, Q., Zha, Z.J., Zhu, Y., Ding, X.: Rain streak removal via dual graph convolutional network. In: Proceedings of the AAAI Conference on Artificial Intelligence. vol. 35, pp. 1352–1360 (2021) [2](#)
18. Gou, W., Yi, Z., Xiang, Y., Li, S., Liu, Z., Kong, D., Xu, K.: Syenet: A simple yet effective network for multiple low-level vision tasks with real-time performance on mobile device. In: Proceedings of the IEEE/CVF International Conference on Computer Vision. pp. 12182–12195 (2023) [11](#)
19. Grainger, R., Paniagua, T., Song, X., Cuntoor, N., Lee, M.W., Wu, T.: Paca-vit: Learning patch-to-cluster attention in vision transformers. In: Proceedings of the IEEE/CVF Conference on Computer Vision and Pattern Recognition. pp. 18568–18578 (2023) [8](#)
20. Guo, J., Han, K., Wu, H., Tang, Y., Chen, X., Wang, Y., Xu, C.: Cmt: Convolutional neural networks meet vision transformers. In: Proceedings of the IEEE/CVF Conference on Computer Vision and Pattern Recognition. pp. 12175–12185 (2022) [8](#)
21. Guo, Q., Sun, J., Juefei-Xu, F., Ma, L., Xie, X., Feng, W., Liu, Y., Zhao, J.: Efficientderain: Learning pixel-wise dilation filtering for high-efficiency single-image deraining. In: Proceedings of the AAAI Conference on Artificial Intelligence. vol. 35, pp. 1487–1495 (2021) [13](#)
22. Guo, S., Yan, Z., Zhang, K., Zuo, W., Zhang, L.: Toward convolutional blind denoising of real photographs. In: Proceedings of the IEEE/CVF conference on computer vision and pattern recognition. pp. 1712–1722 (2019) [2](#), [13](#)
23. Hong, M., Xie, Y., Li, C., Qu, Y.: Distilling image dehazing with heterogeneous task imitation. In: Proceedings of the IEEE/CVF Conference on Computer Vision and Pattern Recognition. pp. 3462–3471 (2020) [13](#)
24. Huang, H., Zhou, X., Cao, J., He, R., Tan, T.: Vision transformer with super token sampling. In: Proceedings of the IEEE/CVF Conference on Computer Vision and Pattern Recognition. pp. 22690–22699 (2023) [8](#)
25. Jaw, D.W., Huang, S.C., Kuo, S.Y.: Desnowgan: An efficient single image snow removal framework using cross-resolution lateral connection and gans. IEEE Transactions on Circuits and Systems for Video Technology **31**(4), 1342–1350 (2020) [13](#)
26. Jiang, K., Wang, Z., Yi, P., Chen, C., Huang, B., Luo, Y., Ma, J., Jiang, J.: Multi-scale progressive fusion network for single image deraining. In: Proceedings of the IEEE/CVF conference on computer vision and pattern recognition. pp. 8346–8355 (2020) [13](#)
27. Jiang, Y., Gong, X., Liu, D., Cheng, Y., Fang, C., Shen, X., Yang, J., Zhou, P., Wang, Z.: Enlightengan: Deep light enhancement without paired supervision. IEEE transactions on image processing **30**, 2340–2349 (2021) [13](#)
28. Jin, Y., Yang, W., Tan, R.T.: Unsupervised night image enhancement: When layer decomposition meets light-effects suppression. In: European Conference on Computer Vision. pp. 404–421. Springer (2022) [13](#)
29. Kim, K., Lee, S., Cho, S.: Mssnet: Multi-scale-stage network for single image deblurring. In: European Conference on Computer Vision. pp. 524–539. Springer (2022) [2](#), [18](#), [19](#)

30. Kim, Y., Soh, J.W., Park, G.Y., Cho, N.I.: Transfer learning from synthetic to real-noise denoising with adaptive instance normalization. In: Proceedings of the IEEE/CVF conference on computer vision and pattern recognition. pp. 3482–3492 (2020) [13](#)
31. Kupyn, O., Budzan, V., Mykhailych, M., Mishkin, D., Matas, J.: Deblurgan: Blind motion deblurring using conditional adversarial networks. In: Proceedings of the IEEE conference on computer vision and pattern recognition. pp. 8183–8192 (2018) [13](#), [18](#)
32. Kupyn, O., Martyniuk, T., Wu, J., Wang, Z.: Deblurgan-v2: Deblurring (orders-of-magnitude) faster and better. In: Proceedings of the IEEE/CVF international conference on computer vision. pp. 8878–8887 (2019) [13](#), [18](#)
33. Li, B., Ren, W., Fu, D., Tao, D., Feng, D., Zeng, W., Wang, Z.: Benchmarking single-image dehazing and beyond. *IEEE Transactions on Image Processing* **28**(1), 492–505 (2018) [11](#), [15](#)
34. Li, B., Liu, X., Hu, P., Wu, Z., Lv, J., Peng, X.: All-in-one image restoration for unknown corruption. In: Proceedings of the IEEE/CVF Conference on Computer Vision and Pattern Recognition. pp. 17452–17462 (2022) [5](#), [11](#)
35. Li, R., Tan, R.T., Cheong, L.F.: All in one bad weather removal using architectural search. In: Proceedings of the IEEE/CVF conference on computer vision and pattern recognition. pp. 3175–3185 (2020) [2](#), [5](#)
36. Li, Y., Fan, Y., Xiang, X., Demandolx, D., Ranjan, R., Timofte, R., Van Gool, L.: Efficient and explicit modelling of image hierarchies for image restoration. In: Proceedings of the IEEE/CVF Conference on Computer Vision and Pattern Recognition. pp. 18278–18289 (2023) [5](#), [11](#)
37. Liang, M., Yang, B., Wang, S., Urtasun, R.: Deep continuous fusion for multi-sensor 3d object detection. In: Proceedings of the European conference on computer vision (ECCV). pp. 641–656 (2018) [2](#)
38. Liu, Y.F., Jaw, D.W., Huang, S.C., Hwang, J.N.: Desnownet: Context-aware deep network for snow removal. *IEEE Transactions on Image Processing* **27**(6), 3064–3073 (2018) [2](#), [13](#)
39. Mou, C., Wang, Q., Zhang, J.: Deep generalized unfolding networks for image restoration. In: CVPR (2022) [4](#), [11](#)
40. Nah, S., Son, S., Lee, S., Timofte, R., Lee, K.M.: Ntire 2021 challenge on image deblurring. In: Proceedings of the IEEE/CVF Conference on Computer Vision and Pattern Recognition. pp. 149–165 (2021) [11](#), [15](#), [16](#), [22](#)
41. Park, D., Kang, D.U., Kim, J., Chun, S.Y.: Multi-temporal recurrent neural networks for progressive non-uniform single image deblurring with incremental temporal training. In: European Conference on Computer Vision. pp. 327–343. Springer (2020) [2](#), [13](#), [18](#)
42. Perera, A.G., Wei Law, Y., Chahl, J.: Uav-gesture: A dataset for uav control and gesture recognition. In: Proceedings of the European Conference on Computer Vision (ECCV) Workshops. pp. 0–0 (2018) [2](#)
43. Prakash, A., Chitta, K., Geiger, A.: Multi-modal fusion transformer for end-to-end autonomous driving. In: Proceedings of the IEEE/CVF Conference on Computer Vision and Pattern Recognition. pp. 7077–7087 (2021) [2](#)
44. Qi, C.R., Liu, W., Wu, C., Su, H., Guibas, L.J.: Frustum pointnets for 3d object detection from rgb-d data. In: Proceedings of the IEEE conference on computer vision and pattern recognition. pp. 918–927 (2018) [2](#)
45. Qin, X., Wang, Z., Bai, Y., Xie, X., Jia, H.: Ffa-net: Feature fusion attention network for single image dehazing. In: Proceedings of the AAAI conference on artificial intelligence. vol. 34, pp. 11908–11915 (2020) [2](#), [13](#), [22](#)

46. Qu, Y., Chen, Y., Huang, J., Xie, Y.: Enhanced pix2pix dehazing network. In: Proceedings of the IEEE/CVF conference on computer vision and pattern recognition. pp. 8160–8168 (2019) [13](#), [22](#)
47. Radford, A., Kim, J.W., Hallacy, C., Ramesh, A., Goh, G., Agarwal, S., Sastry, G., Askell, A., Mishkin, P., Clark, J., et al.: Learning transferable visual models from natural language supervision. In: International conference on machine learning. pp. 8748–8763. PMLR (2021) [9](#)
48. Ren, C., He, X., Wang, C., Zhao, Z.: Adaptive consistency prior based deep network for image denoising. In: Proceedings of the IEEE/CVF conference on computer vision and pattern recognition. pp. 8596–8606 (2021) [2](#), [13](#)
49. Ren, D., Zuo, W., Hu, Q., Zhu, P., Meng, D.: Progressive image deraining networks: A better and simpler baseline. In: Proceedings of the IEEE/CVF conference on computer vision and pattern recognition. pp. 3937–3946 (2019) [2](#), [13](#)
50. Rim, J., Lee, H., Won, J., Cho, S.: Real-world blur dataset for learning and benchmarking deblurring algorithms. In: Computer Vision–ECCV 2020: 16th European Conference, Glasgow, UK, August 23–28, 2020, Proceedings, Part XXV 16. pp. 184–201. Springer (2020) [11](#), [15](#), [16](#), [22](#)
51. Ronneberger, O., Fischer, P., Brox, T.: U-net: Convolutional networks for biomedical image segmentation. In: Medical Image Computing and Computer-Assisted Intervention–MICCAI 2015: 18th International Conference, Munich, Germany, October 5–9, 2015, Proceedings, Part III 18. pp. 234–241. Springer (2015) [3](#), [6](#)
52. Song, Y., He, Z., Qian, H., Du, X.: Vision transformers for single image dehazing. *IEEE Transactions on Image Processing* **32**, 1927–1941 (2023) [13](#), [22](#)
53. Tao, X., Gao, H., Shen, X., Wang, J., Jia, J.: Scale-recurrent network for deep image deblurring. In: IEEE Conference on Computer Vision and Pattern Recognition (CVPR) (2018) [18](#)
54. Tsai, F.J., Peng, Y.T., Lin, Y.Y., Tsai, C.C., Lin, C.W.: Stripformer: Strip transformer for fast image deblurring. In: European Conference on Computer Vision. pp. 146–162. Springer (2022) [13](#), [18](#), [19](#)
55. Tu, Z., Talebi, H., Zhang, H., Yang, F., Milanfar, P., Bovik, A., Li, Y.: Maxim: Multi-axis mlp for image processing. *CVPR* (2022) [5](#), [11](#), [16](#)
56. Valanarasu, J.M.J., Yasarla, R., Patel, V.M.: Transweather: Transformer-based restoration of images degraded by adverse weather conditions. In: Proceedings of the IEEE/CVF Conference on Computer Vision and Pattern Recognition. pp. 2353–2363 (2022) [2](#), [5](#), [11](#), [17](#)
57. Vaswani, A., Shazeer, N., Parmar, N., Uszkoreit, J., Jones, L., Gomez, A.N., Kaiser, Ł., Polosukhin, I.: Attention is all you need. *Advances in neural information processing systems* **30** (2017) [7](#)
58. Wang, H., Chen, X., Ni, B., Liu, Y., Liu, J.: Omni aggregation networks for lightweight image super-resolution. In: Proceedings of the IEEE/CVF Conference on Computer Vision and Pattern Recognition. pp. 22378–22387 (2023) [3](#), [5](#), [7](#)
59. Wang, H., Xie, Q., Zhao, Q., Meng, D.: A model-driven deep neural network for single image rain removal. In: Proceedings of the IEEE/CVF conference on computer vision and pattern recognition. pp. 3103–3112 (2020) [13](#)
60. Wang, W., Wei, C., Yang, W., Liu, J.: Gladnet: Low-light enhancement network with global awareness. In: 2018 13th IEEE international conference on automatic face & gesture recognition (FG 2018). pp. 751–755. IEEE (2018) [2](#), [13](#)
61. Wang, Z., Cun, X., Bao, J., Zhou, W., Liu, J., Li, H.: Uformer: A general u-shaped transformer for image restoration. In: Proceedings of the IEEE/CVF Conference on Computer Vision and Pattern Recognition (CVPR). pp. 17683–17693 (June 2022) [4](#), [11](#)

62. Wei, C., Wang, W., Yang, W., Liu, J.: Deep retinex decomposition for low-light enhancement. arXiv preprint arXiv:1808.04560 (2018) [11](#), [15](#), [16](#)
63. Wu, H., Qu, Y., Lin, S., Zhou, J., Qiao, R., Zhang, Z., Xie, Y., Ma, L.: Contrastive learning for compact single image dehazing. In: Proceedings of the IEEE/CVF Conference on Computer Vision and Pattern Recognition. pp. 10551–10560 (2021) [2](#), [13](#), [22](#)
64. Yang, W., Tan, R.T., Feng, J., Liu, J., Guo, Z., Yan, S.: Deep joint rain detection and removal from a single image. In: Proceedings of the IEEE conference on computer vision and pattern recognition. pp. 1357–1366 (2017) [13](#)
65. Ye, Y., Chang, Y., Zhou, H., Yan, L.: Closing the loop: Joint rain generation and removal via disentangled image translation. In: Proceedings of the IEEE/CVF conference on computer vision and pattern recognition. pp. 2053–2062 (2021) [2](#), [13](#)
66. Yue, Z., Yong, H., Zhao, Q., Meng, D., Zhang, L.: Variational denoising network: Toward blind noise modeling and removal. *Advances in neural information processing systems* **32** (2019) [13](#)
67. Yue, Z., Zhao, Q., Zhang, L., Meng, D.: Dual adversarial network: Toward real-world noise removal and noise generation. In: Computer Vision–ECCV 2020: 16th European Conference, Glasgow, UK, August 23–28, 2020, Proceedings, Part X 16. pp. 41–58. Springer (2020) [13](#)
68. Zamir, S.W., Arora, A., Khan, S., Hayat, M., Khan, F.S., Yang, M.H.: Restormer: Efficient transformer for high-resolution image restoration. In: Proceedings of the IEEE/CVF conference on computer vision and pattern recognition. pp. 5728–5739 (2022) [3](#), [7](#), [11](#), [16](#), [17](#)
69. Zamir, S.W., Arora, A., Khan, S., Hayat, M., Khan, F.S., Yang, M.H., Shao, L.: Learning enriched features for real image restoration and enhancement. In: Computer Vision–ECCV 2020: 16th European Conference, Glasgow, UK, August 23–28, 2020, Proceedings, Part XXV 16. pp. 492–511. Springer (2020) [13](#)
70. Zamir, S.W., Arora, A., Khan, S., Hayat, M., Khan, F.S., Yang, M.H., Shao, L.: Multi-stage progressive image restoration. In: CVPR (2021) [4](#), [11](#)
71. Zhang, H., Dai, Y., Li, H., Koniusz, P.: Deep stacked hierarchical multi-patch network for image deblurring. In: Proceedings of the IEEE/CVF Conference on Computer Vision and Pattern Recognition. pp. 5978–5986 (2019) [13](#), [18](#)
72. Zhang, K., Zuo, W., Chen, Y., Meng, D., Zhang, L.: Beyond a gaussian denoiser: Residual learning of deep cnn for image denoising. *IEEE transactions on image processing* **26**(7), 3142–3155 (2017) [2](#)
73. Zhang, K., Li, R., Yu, Y., Luo, W., Li, C.: Deep dense multi-scale network for snow removal using semantic and depth priors. *IEEE Transactions on Image Processing* **30**, 7419–7431 (2021) [2](#), [13](#)
74. Zhang, K., Luo, W., Zhong, Y., Ma, L., Stenger, B., Liu, W., Li, H.: Deblurring by realistic blurring. In: Proceedings of the IEEE/CVF Conference on Computer Vision and Pattern Recognition. pp. 2737–2746 (2020) [2](#), [13](#), [18](#)
75. Zhang, Y., Zhang, J., Guo, X.: Kindling the darkness: A practical low-light image enhancer. In: Proceedings of the 27th ACM international conference on multimedia. pp. 1632–1640 (2019) [13](#)
76. Zhu, J.Y., Park, T., Isola, P., Efros, A.A.: Unpaired image-to-image translation using cycle-consistent adversarial networks. In: Proceedings of the IEEE international conference on computer vision. pp. 2223–2232 (2017) [13](#)